Investigation of signal extraction in the frame of laser induced breakdown spectroscopy imaging

Vincent Motto-Ros, S. Moncayo, F. Trichard, F. Pelascini

Investigation of signal extraction in the frame of LIBS imaging

V. Motto-Ros[1*], S. Moncayo[1], F. Trichard[2], F. Pelascini[3]

[1] *Institut Lumière Matière UMR 5306, Université Lyon 1 - CNRS, Université de Lyon 69622 Villeurbanne, France*

[2]*Ablatom S.A.S, Bâtiment Kastler, Domaine Scientifique de la Doua, 10 rue Ada Byron, 69622 Villeurbanne Cedex, France*

[3]*Cetim Grand Est 67305 Schiltigheim, France*

Keywords: LIBS, Elemental Imaging, Line Intensity Extraction

Highlights

- This paper focuses on the evaluation of various intensity extraction methods for LIBS-based imaging.
- Based on a statistical evaluation, we show the possibility of associating uncertainty with each extracted value.
- A conditional extraction method is proposed based on this uncertainty estimation.

Abstract

Laser-induced breakdown spectroscopy (LIBS)-based imaging techniques have become well known among spatially resolved elemental approaches due to their mature instrumentation and outstanding advantages and applications. Data processing and in particular signal extraction are key in all LIBS-based imaging analyses to provide robust and reliable results. To date, there has not been a statistical evaluation of this issue when processing large and complex LIBS datasets. In this work, we aimed to test the performance of three extraction methods applied to micro-LIBS-based imaging. We also proposed a new conditional data extraction procedure relying on the statistical uncertainty associated with the extracted signal. We built a synthetic spectral dataset with controlled spectral features and tested the linearity, dynamic range and operating speed of different extraction approaches. The results of this study demonstrate the importance of data extraction and provide evidence for its optimization. This procedure is of particular relevance for the extraction of weak line intensities and in cases where the presence or absence of certain elements is critical (i.e., biomedical applications or trace analysis). In addition, the proposed conditional approach offers new insights into the means of providing LIBS imaging results.

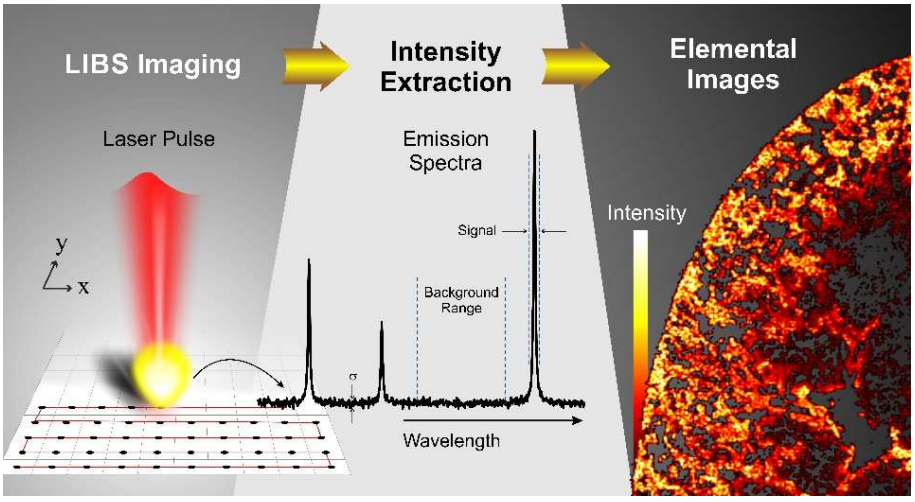

Abstract figure

1. Introduction

In the last few years, the application of laser-induced breakdown spectroscopy (LIBS) to elemental imaging has attracted increasing attention and is currently a promising axis for LIBS development. In LIBS-based imaging, a laser-induced plasma is generated at each position of the sample surface covering the region to be analyzed. After extracting the line intensities associated with the elements of interest from each recorded spectrum, elemental maps are then built to obtain the corresponding elemental images [1-5]. Compared to other spatially resolved techniques, LIBS-based imaging offers several advantages, such as table-top instrumentation, ease of use, speed of operation, detection of light elements, micrometer spatial resolution and accessible limit of detection (LOD) at the ppm level [4, 6]. Among the panel of spatially resolved elemental approaches, this approach has demonstrated its potential to become a reference technique by providing successful results in various fields of application, including geological studies [4, 5, 7-10], industrial applications [11-15], and biomedical analysis [16-21].

Although LIBS-based imaging technology and instrumentation are currently mature, the challenging task of processing large spectral datasets remains vaguely explored. New developments and solutions in these aspects are still required. LIBS imaging spectral datasets share features and problems with multispectral imaging approaches [22]. Each spectrum (i.e., pixel) of the image may be defined by a large number of intensity channels, and difficulties arise in extracting and representing the more relevant information of a spectral dataset. Additionally, LIBS imaging experiments are carried out in single-shot mode. The spectra are then generally noisy, and the signal to be extracted is close to the baseline level. In addition, the large amount of data generated does not allow manual processing of spectra, and extraction procedures able to work in an unsupervised manner and to ensure reliable results are needed.

Despite the large amount of literature published on LIBS-based imaging and the importance of data processing, very few studies have considered the influence of data extraction procedures on the quality of LIBS imaging results. To date, aspects regarding data extraction have only been reported in conventional macro-LIBS [23-26]. Our group has proposed several data processing strategies adapted to the megapixel LIBS-based imaging of single- and multiphase materials [4, 21, 27]. Other approaches based on the use of chemometrics have also been reported by several groups with promising results for the future [28-31].

To the best of our knowledge, there are no results in the literature focusing on data extraction procedures applied to micro-LIBS-based imaging. Here, we aim to evaluate the quality and robustness of different extraction methods applied to micro-LIBS-based imaging and to assess a new data extraction procedure based on a conditional threshold criterion. The original idea introduced in this manuscript consists of working with synthetic spectral datasets that are built with controlled spectral features (line intensity, line shape, and noise) and then evaluating the extraction methods in terms of sensitivity to noise, dynamic range and processing speed. Additionally, we also estimate the statistical uncertainty of the extracted signals and assess a conditional extraction approach for both synthetic and real LIBS images.

2. Materials and methods

2.1. Preamble

When performing a LIBS imaging experiment, it is common to wonder whether a specific pixel is just noise or whether it represents a significant signal. This point is critical in the case of analyzing trace elements and samples that produce weak signals, as occurs, for instance, in many biomedical applications. Currently, the answer is subjective: the spectrum corresponding to such a pixel has to be manually explored, and the analyst will eventually make the decision

based on his/her experience. Under these conditions, the validity of the result may be questioned, which represents a weakness of the method. To validate a LIBS image and the intensities reported in each pixel, the first aspect to be evaluated is the extraction procedures that can be applied. As mentioned above, data extraction has to be unsupervised, and it should operate as fast as possible and ideally cover a large dynamic range (from trace to major emission lines). To assess such extraction procedures, our first idea was to analyze a homogenous sample (with known elemental concentrations), then apply different extraction methods to the collected spectra and evaluate their figure of merits. This approach is however not possible, because such evaluation requires to know in advance the line intensity that should be extracted. In practice, there are operational issues such as the shot-to-shot fluctuations of the laser pulse energy, the sample flatness and possible surface contaminations, and more importantly the heterogeneity of sample itself. It is indeed difficult, if not impossible, to design a material rigorously homogenous at the scale of the laser spot (~ 5 µm in our case).

To overcome this constraint, we created a synthetic dataset from a dummy image where the intensity of and noise associated with each pixel were known. We obtained an experimental spectrum to simulate a synthetic dataset as close as possible to an experimental dataset (i.e., same line shape and width, similar noise level, etc.). Then, we applied different extraction algorithms to evaluate their performances. Notably, this dataset applies to a simple spectrum with isolated emission lines (free from interferences) and a simple continuum structure, as normally found in most of our numerous biological specimens, calcium carbonate samples, aluminum-based matrices and so on [5, 6, 11, 14].

2.2. Experimental spectrum

The general protocol and the LIBS instrument used for this study have already been described in previous reports [5, 6, 32]. Briefly, we used an IR laser pulse energy of 1 mJ with

a laser spot size of approximately 8 µm, and plasma emission was analyzed by using a 300 mm focal length Czerny-Turner spectrometer (Shamrock 303, Andor Technology) coupled to an ICCD camera (Istar, Andor Technology). The spectrum was obtained with 1 µs of delay time, a time-width gate of 3 µs, an ICCD gain of 1500 and argon gas flowing through the plasma region. Our spectrometer was equipped with a 1800 l/mm holographic grating, allowing a spectral range of approximately 20 nm to be covered. The entrance slit of the spectrometer was set to 30 µm. With this configuration, the spectral resolution was 0.08 nm, and the distance between two consecutive points (i.e., spectral channels) was 0.023 nm.

We recorded a single-shot spectrum from a reference sample containing 50 ppm zinc in an epoxy matrix (cf. figure 1). From this spectrum, we retrieved the spectral information required to simulate the synthetic dataset: the line shape can be considered a Lorentzian profile; the continuum emission was constant in the probed spectral range; and the noise follows a Gaussian distribution with a standard deviation of 170 counts. The last of these three points shows that when the line intensities are weak (i.e., close to the background value), the spectral noise can be considered independent of the intensity level [33]. We will make this assumption in all the following studies.

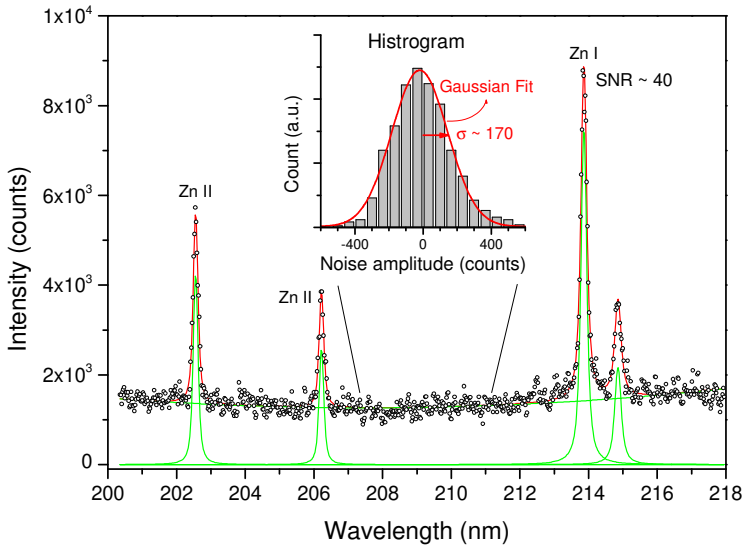

Figure 1: Single-shot spectrum from a reference sample containing 50 ppm zinc in an epoxy matrix (dotted plot). A fit (red curve) was obtained using four individual Lorentz profiles and a polynomial baseline (green curves). The inset shows the histogram of spectral noise retrieved from the fit residue, which follows a normal distribution.

2.3. Synthetic spectral dataset

By keeping the spectral features of our experimental Zn spectrum, we simulated a series of spectra for nine different intensity levels (net intensity of Zn I at 213.86 nm) defined from 4 to 1024 in arbitrary units (a.u.). We added a constant continuum value of 100 a.u. and random Gaussian noise with a standard deviation of 8 a.u. (figure 2a). This synthetic dataset was simulated from the square image shown in figure 2b, defined by 450x450 pixels. This image is composed of nine levels of intensities that result in a dynamic range extending from 0.5 to 128 in terms of SNR. A zone of the image with a constant intensity level (i.e., the different colors in figure 2b) corresponds to a rectangle of 450 x 50 pixels. As we will see in the following, the 22 500 pixels contained in each rectangle allow evaluation of the average extracted intensity as well as its associated standard deviation.

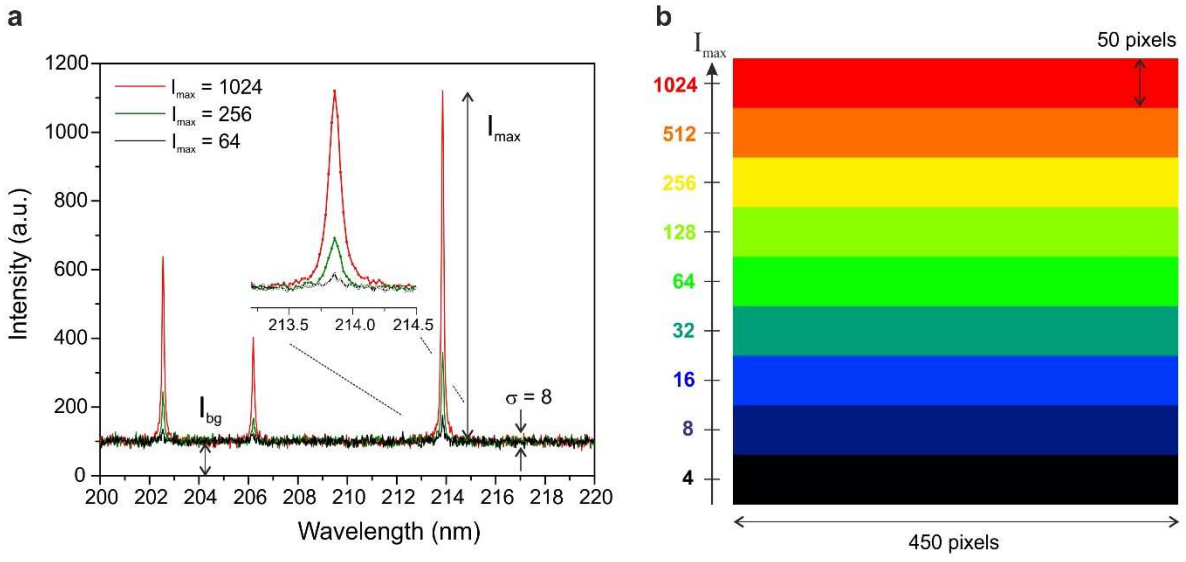

Figure 2: a) Simulated spectra for I_{max}=1024, 256, and 64 a.u. b) Synthetic image containing 9 levels of intensities, varying from 4 to 1024 a.u.

2.4. Extraction methods

We considered three different methods for extracting the line intensities from LIBS spectra as detailed hereafter and summarized in figure 3. The method description, baseline calculation and extraction speed are also given in table 1. These three selected methods were chosen to fulfill the requirements in terms of speed imposed by LIBS imaging: they all have an extraction speed above 1000 spectra processed per second (cf. table 1). These values were estimated in the LabVIEW environment using a personal laptop configured with an Intel core i9 processor and 32 GB of RAM. For instance, spectral fitting by using Lorentzian, Gaussian or Voigt profiles is not adequate, as it is relatively slow (approximately 10 spectrum/second) and requires human supervision to avoid the possible divergence of the fitting algorithm.

The first selected method (E_1) is based on a simple intensity subtraction I_{max}-I_{min}, where I_{min} and I_{max} are respectively the minimum and maximum intensities in a predefined spectral range. The second (E_2) is also based on the subtraction I_{peak}-I_{min}, in which I_{min} is defined as the value of the baseline estimated from a polynomial fit in a spectral window close to I_{peak}. I_{peak} is retrieved from a peak detection algorithm that uses the second derivative of the line shape (Peak Detector VI, LabVIEW). The spectral ranges in both E_1 and E_2 were defined by the analyst as corresponding to tenfold the line width for each side, and the signal corresponds to the net peak intensity. Finally, the third extraction method (E_3) used two spectral windows defined by the analyst covering the line of interest and the surrounding background, respectively. The line area can then be calculated by Eq. 1:

$$I_S = \sum_{i=1}^{n_S} I_i - n_S\overline{I_{BG}}, \quad (1)$$

where n_S and n_{bg} represent the number of points in the signal and background windows, respectively, and $\overline{I_{BG}}$ the average value of the background within n_{bg}.

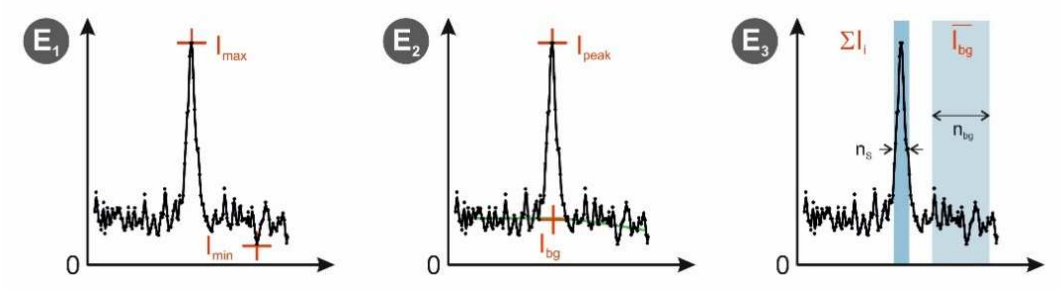

Figure 3: Description of the three methods of data extraction (labeled from 1 to 3) evaluated. Methods E_1 and E_2 are based on the extraction of the intensity of the line, while methods E_3 is based on the calculation of the peak area.

Table 1: Features of the three investigated extraction methods.

Method	Description	Baseline	Extraction speed (spectra/seg)
E_1	Max – Min	Punctual	32 000
E_2	Peak Detection	Polynomial fit $n = 2$	5 000
E_3	Peak Area	Averaged	28 000

3. Results

3.1. Evaluation of the extraction methods

We applied the three extraction algorithms to retrieve the net intensity (E_1 and E_2) and line area (E_3) of the Zn I line and to convert it into a matrix displayed as an image by a false color scale. A portion of the extracted image is shown for E1, E2, E3 and the original image in figure 4a. The 22 500 spectra (450 x 50 pixels) contained at each intensity level were used to calculate

the average extracted intensity and its associated standard deviation. Figure 4b shows the averaged extracted intensities and the corresponding expected value. E_1 showed an important bias for spectra with SNR values below 20, as it was highly sensitive to noise and thus was not adequate when dealing with weak line intensities. Indeed, the observed bias was mainly produced by the extraction of the background I_{min}. However, to a lesser extent, E_2 was also affected by spectral noise. This effect became important for those spectra with an SNR lower than eight. The polynomial baseline fitting reduced the uncertainty in the estimation of I_{min} compared to E_1. However, this algorithm uses 60% of the lowest values to perform the polynomial fit, which may have induced an underestimation of the background. Moreover, for weak emission lines, the peak detection algorithm was not always able to find the maximum, causing inaccuracies in the I_{max} determination. In contrast, E_3 showed a linear correlation within the whole dynamical range and was able to accurately extract the intensity values even with low SNR spectra. E_3 intensity values were rescaled by a factor of 0.14 (ratio between the line maximum and the line area) to display the three extraction outputs on the same graph. In the following, we aimed to optimize the E_3 method by investigating the effect of modifying n_{bg} and n_S.

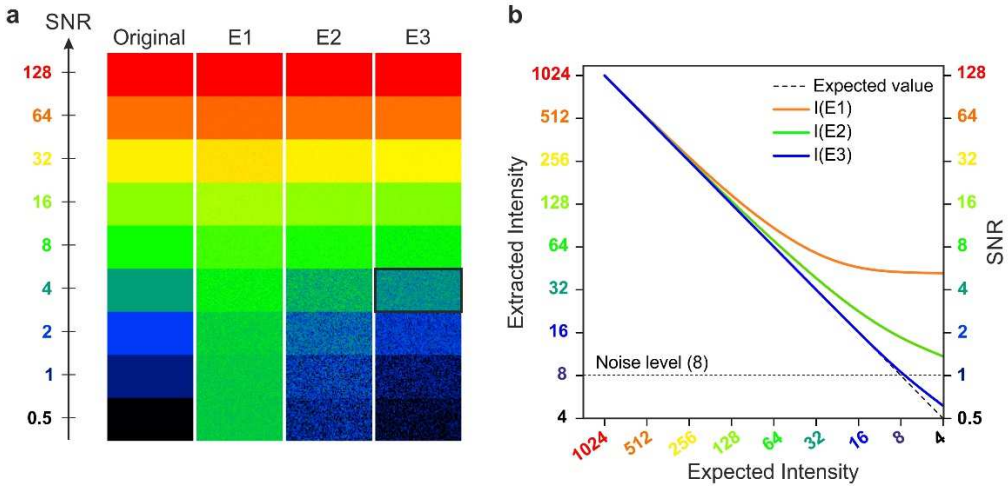

Figure 4: Extraction results of the three selected methods. The reported intensity values are expressed in arbitrary units. a) Portion of the extracted images. b) Evolution of the extracted averaged intensities.

3.2. Uncertainty and optimization of the extraction method E_3

As shown above, method E_3 did not introduce any bias; therefore, using Eq. 1 and considering the same standard deviation (σ) from the emission the line of interest and the background, it is possible to determine a statistical uncertainty (u_S) associated with each extracted value (I_S) by Eq. 2:

$$u_S{}^2 = \left(\frac{\sigma \times n_S}{\sqrt{n_S}}\right)^2 + \left(n_S \times \frac{\sigma}{\sqrt{n_{BG}}}\right)^2 = (n_s \times \sigma)^2 \left(\frac{1}{n_S} + \frac{1}{n_{BG}}\right) \quad (2)$$

This uncertainty may be represented as a function of the number of points that encompasses the continuum and the signal windows used, n_{BG} and n_S, respectively. The influence on u_S of both n_{BG} and n_S is shown in figure 5 in the case of an SNR of 32. Figure 5a represents a single spectrum in the range of the Zn I line of interest. The signal window Δλ (associated with n_S) and the full width at half maximum of the emission line (δλ) are also indicated. Figure 5b presents the signal uncertainty, calculated as $u_{rel}(\%) = u_S/I_S$, for two n_S values, 7 and 17, and varying n_{BG}. The plain curves represent the u_S model, as determined from Eq. 2, and the points are the relative standard deviations extracted from the image shown in figure 4 for the SNR value of 32 (yellow rectangle). Both show good agreement, confirming the validity of Eq. 2 for estimating the statistical fluctuations related to extraction. In addition, the number of points used to estimate the background had a strong influence on u_S. Background windows smaller than 2 nm (i.e., $n_{bg} \sim 87$ points) resulted in larger u_S values, whereas for larger background widths, the uncertainty tended to a constant and minimal value. Regardless of the n_S considered, we observed a similar curve trend; however, the smaller the value of n_S is, the lower the u_S

value. The influence of n_S is represented more accurately in figure 5c. This graph represents the signal uncertainty obtained by fixing three different n_{BG} values and modifying the number of points used to extract the signal. Here, we observed an opposite effect: increasing n_S resulted in a larger uncertainty value. This phenomenon is due to the average value of continuum $\overline{I_{BG}}$ that has to be subtracted n_S times from the signal $\sum_{i=1}^{n_S} I_i$ (Eq. 1), thus enhancing the effect of the background noise. At $n_S \sim 5$, the u_{rel} reaches a minimum, and this optimal value corresponds to $\Delta\lambda/\delta\lambda \sim 1$.

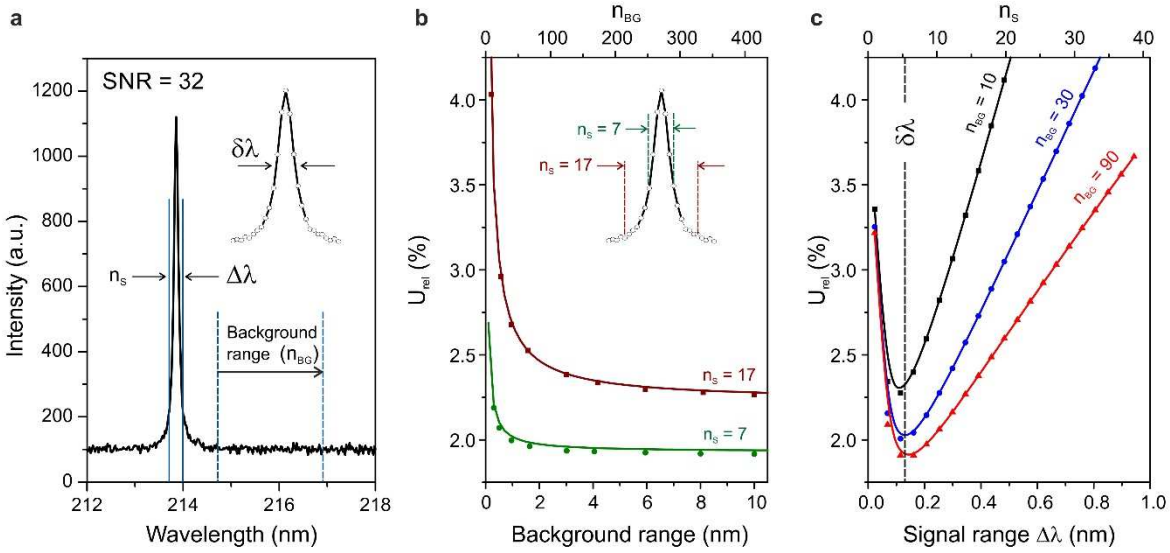

Figure 5: Uncertainties associated with E_3 as a function of both spectral windows for the SNR = 32. a) Definition of both spectral windows, where $\delta\lambda$ is the full width at half maximum of the emission line. b) Influence of the background range for $n_S = 5$ and $n_S = 17$ on u_{rel}. c) Influence of the signal range for $n_{BG} = 10$, 30, and 90 on u_{rel}.

3.3. Conditional extraction data processing

The possibility of estimating the statistical uncertainty associated with each extracted signal opens interesting perspectives for LIBS imaging data processing. For instance, we can create a

conditional extraction method able to discriminate statistically relevant pixels corresponding to real signals from those containing noise. This discrimination process can be defined on the basis of the definition of the limit of detection (LOD). The LOD is generally considered the ultimate concentration at which it is possible to provide statistical evidence of the presence of an analyte [34, 35]. Similarly, in analytical methods where the concentration is obtained by interpolating an unknown spectral intensity in a calibration curve, the 3σ approach is widely adopted to calculate the LOD. In this approach, the LOD is defined as three times the standard deviation of the background measured at the close vicinity of the line of interest, considering a normal distribution of noise and α = 0.05 at the statistical level.

In an equivalent manner, instead of using the conventional 3 x σ for defining the minimum significant signal, we considered here k x u_s with k = 3 as the lowest significant extracted intensity. Therefore, those spectra with an I_s lower than 3 x u_s will not be considered, and their pixel value in the image is set arbitrarily to 0.

To evaluate this conditional approach, we selected a well-known image of A. Einstein (cf. figure 6a) composed of 500 x 500 pixels and containing 256 different levels of intensities (from 0 to 255). Based on this image, as previously described, we created a second synthetic series of spectra by adding the same random Gaussian noise (i.e., $\sigma = 8$ a.u.). In this dataset, the net line intensity of the different simulated spectra extends from 0 to 255 according to each pixel value of the image. Figure 6b shows the same image, but all pixels with intensity values below $3 \times \sigma$ are now displayed in red, following the conventional LOD definition discussed above. In this case, 37% of pixels are not statistically significant (proportion of red pixels in the entire image). Note that pixels of the image having an actual 0 value are displayed in yellow; however, their numbers are not significant enough to consider them in the following. As shown in figure 6c, when applying the peak surface method (E_3) combined with the conditional rule described

above, the detection capability improves, and the percentage of significant signals increases (only 27% of pixels are not significant). The improvement factor was estimated to be approximately 3 when using optimal settings of n_S and n_{BG}. Therefore, this extraction method allows extraction of a significant signal for a line intensity corresponding to an SNR=1.

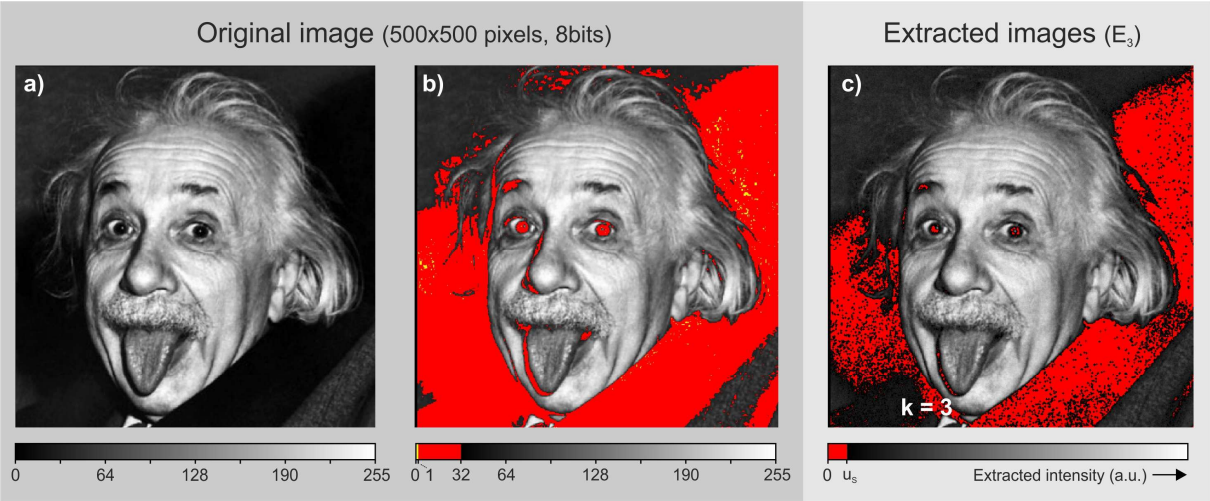

Figure 6: Example of conditional extraction. a) Original 8-bit image of 500x500 pixels used to build a synthetic dataset. b) Same image as that in a) with all the pixels lower than (3 x σ) displayed in red considering σ = 8 a.u. c) Image obtained when applying the conditional extraction method E_3 with a confidence level k = 3 to the synthetic dataset.

3.4. Application to a real LIBS-based image

Finally, we demonstrated the advantages of applying the peak surface method (E_3) and the proposed conditional approach in a real LIBS-based image. We selected an experimental dataset obtained to determine the gadolinium (Gd) level in a section of a murine kidney [36]. Figure 7 shows the Gd image (Gd II 342.247 nm) extracted by applying method E_3 (left panel) and the image of the relative uncertainty, u_s (%), calculated for each pixel (right panel). This dataset consists of 80 000 individual spectra. The determination of $u_s$was performed for each

individual spectrum by estimating its baseline noise (σ) in the windows used to extract the background value $\overline{I_{BG}}$. The extracted intensity I_S was then conditionally evaluated as described above. This extraction was conducted in a completely unsupervised manner, and the 80 000 spectra were processed in approximately 6 seconds. Due to the additional operations performed by the algorithm (determination of σ, calculation of u_s, and conditional evaluation), compared to the value reported in table 1, the extraction speed was indeed reduced. However, the current extraction speed (i.e., ~14 000 spectra / second) remains completely acceptable.

The combination of LIBS elemental images with their corresponding uncertainty image is of paramount importance to ensure the quality and accuracy of results. The proposed data processing methodology eliminates the subjective decision by uniquely relying on statistics. In summary, our results shed light on data processing aspects and provide new tools to strengthen LIBS-based imaging development.

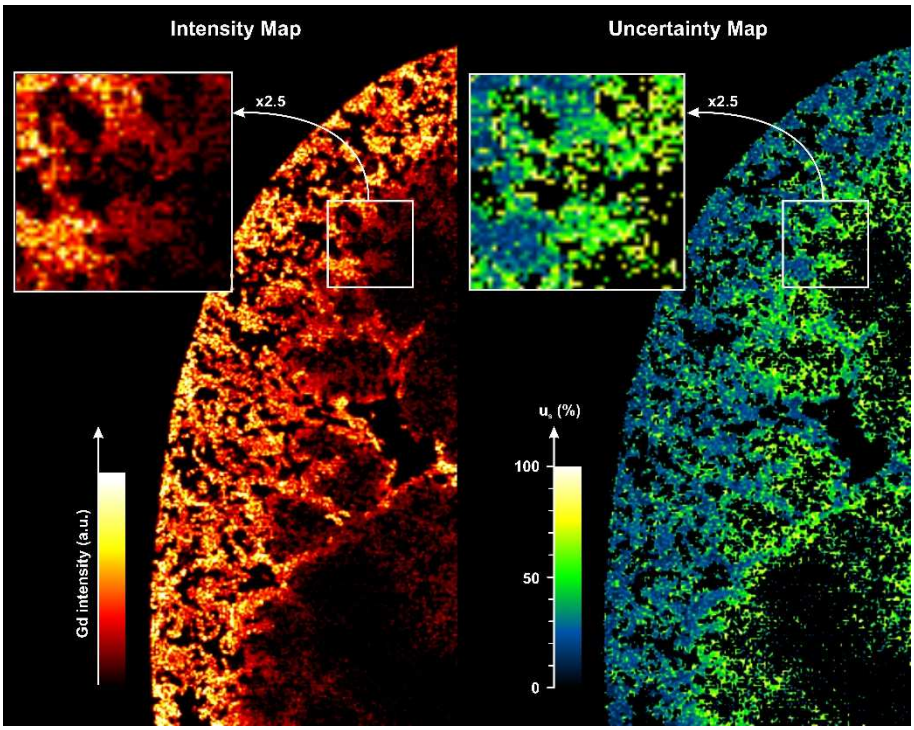

Figure 7: Elemental images of Gd distribution in a murine kidney with a 10 µm spatial resolution and a sequence of 200x400 pixels [36]. a) Intensity images extracted by using E_3. b) Associated relative uncertainty image expressed in %.

4. Conclusion

Here, we studied the influence of three data extraction procedures on the quality of micro-LIBS-based imaging by evaluating their performance and robustness. One of the most remarkable results was that the use of two spectral windows covering the line of interest and the surrounding background (E_3) provided the best extraction performance in terms of linearity, dynamic range and processing speed. We noticed that E_3 not only was perfectly suitable to process large LIBS-based imaging datasets for lines that present a low SNR but also remains robust for strong emission lines. We also proposed a method to estimate the uncertainty associated with an extracted line intensity in a single-shot LIBS-based imaging experiment. Our results indicated that the number of points that covers each spectral window, n_{BG} and n_S, had a key influence on the uncertainty degree and had to be optimized for each emission line. In practice, we may consider a background range covering one or two nanometers ($n_{BG} \sim 50$ in our case) as ideal, whereas the width of the signal window should be restricted to the points corresponding to the half maximum of the emission line ($n_S = 5$ in our case).

Based on the uncertainty associated with each pixel image, we proposed a conditional data processing approach able to provide the best line intensity extraction and to display only those pixels that are statistically significant in a robust, fast and unsupervised manner. Compared to conventional data extraction, this method provides threefold detection capability and enables the successful extraction of emission lines with an SNR close to one. The confidence level k

can be set arbitrarily according to the application; this ability is of particular interest when the presence/absence of an element in the image implies important decisions to be made.

This work also opens new perspectives progressing towards quantitative LIBS imaging. The possibility of providing an estimation of the uncertainty associated with single-shot analysis may represent a step forward for developing models able to address quantitative analysis. In practice, different ablated masses and/or plasma parameters (N_e, T) produced by shot-to-shot variations and different physical and chemical properties (i.e., roughness, composition) within samples are important sources of uncertainty to be considered as well. Further studies dedicated to these issues need to be conducted.

Acknowledgements

This work was partially supported by Pulsalys (#L0978-L1294), the French region Rhônes Alpes Auvergne (Optolyse, CPER2016), the French region Grand Est, and the French ANR (projects MediLIBS and Imazinc).

5. References

[1] M.P. Mateo, G. Nicolas, Laser-Induced Breakdown Spectroscopy for Chemical Mapping of Materials AU - Piñon, V, App. Spectrosc. Rev. 48 (2013) 357-383.

[2] L. Jolivet, M. Leprince, S. Moncayo, L. Sorbier, C.P. Lienemann, V. Motto-Ros, Review of the recent advances and applications of LIBS-based imaging, Spectrochim. Acta Part B 151 (2019) 41-53.

[3] B. Busser, S. Moncayo, J.-L. Coll, L. Sancey, V. Motto-Ros, Elemental imaging using laser-induced breakdown spectroscopy: A new and promising approach for biological and medical applications, Coord. Chem. Rev. 358 (2018) 70-79.

[4] C. Fabre, D. Devismes, S. Moncayo, F. Pelascini, F. Trichard, A. Lecomte, B. Bousquet, J. Cauzid, V. Motto-Ros, Elemental imaging by laser-induced breakdown spectroscopy for the geological characterization of minerals, J. Anal. At. Spectrom. 33 (2018) 1345-1353.

[5] J.O. Cáceres, F. Pelascini, V. Motto-Ros, S. Moncayo, F. Trichard, G. Panczer, A. Marín-Roldán, J.A. Cruz, I. Coronado, J. Martín-Chivelet, Megapixel multi-elemental imaging by Laser-Induced Breakdown Spectroscopy, a technology with considerable potential for paleoclimate studies, Sci. Rep. 7 (2017) 5080.

[6] L. Sancey, V. Motto-Ros, B. Busser, S. Kotb, J.M. Benoit, A. Piednoir, F. Lux, O. Tillement, G. Panczer, J. Yu, Laser spectrometry for multi-elemental imaging of biological tissues, Sci. Rep. 4 (2014) 6065.

[7] F. Trichard, S. Moncayo, D. Devismes, F. Pelascini, J. Maurelli, A. Feugier, C. Sasseville, F. Surma, V. Motto-Ros, Evaluation of a compact VUV spectrometer for elemental imaging by laser-induced breakdown spectroscopy: application to mine core characterization, J. Anal. At. Spectrom 32 (2017) 1527-1534.

[8] C. Gottlieb, S. Millar, S. Grothe, G. Wilsch, 2D evaluation of spectral LIBS data derived from heterogeneous materials using cluster algorithm, Spectrochim. Acta Part B 134 (2017) 58-68.

[9] K. Rifai, F. Doucet, L. Özcan, F. Vidal, LIBS core imaging at kHz speed: Paving the way for real-time geochemical applications, Spectrochim. Acta Part B 150 (2018) 43-48.

[10] L. Bassel, V. Motto-Ros, F. Trichard, F. Pelascini, F. Ammari, R. Chapoulie, C. Ferrier, D. Lacanette, B. Bousquet, Laser-induced breakdown spectroscopy for elemental characterization of calcitic alterations on cave walls, Environ. Sci. Pollut. Res. Int. 24 (2017) 2197-2204.

[11] G. Alombert-Goget, F. Trichard, H. Li, C. Pezzani, M. Silvestre, N. Barthalay, V. Motto-Ros, K. Lebbou, Titanium distribution profiles obtained by luminescence and LIBS measurements on Ti: Al2O3 grown by Czochralski and Kyropoulos techniques, Opt. Mat. 65 (2017) 28-32.

[12] F. Boué-Bigne, Laser-induced breakdown spectroscopy applications in the steel industry: Rapid analysis of segregation and decarburization, Spectrochim. Acta Part B 63 (2008) 1122-1129.

[13] X. Wang, V. Motto-Ros, G. Panczer, D. De Ligny, J. Yu, J.M. Benoit, J.L. Dussossoy, S. Peuget, Mapping of rare earth elements in nuclear waste glass–ceramic using micro laser-induced breakdown spectroscopy, Spectrochim. Acta Part B 87 (2013) 139-146.

[14] F. Trichard, F. Gaulier, J. Barbier, D. Espinat, B. Guichard, C.-P. Lienemann, L. Sorbier, P. Levitz, V. Motto-Ros, Imaging of alumina supports by laser-induced breakdown spectroscopy: A new tool to understand the diffusion of trace metal impurities, J. Catal. 363 (2018) 183-190.

[15] C.M. Ahamer, K.M. Riepl, N. Huber, J.D. Pedarnig, Femtosecond laser-induced breakdown spectroscopy: Elemental imaging of thin films with high spatial resolution, Spectrochim. Acta Part B 136 (2017) 56-65.

[16] B. Busser, S. Moncayo, F. Trichard, V. Bonneterre, N. Pinel, F. Pelascini, P. Dugourd, J.L. Coll, M. D'Incan, J. Charles, V. Motto-Ros, L. Sancey, Characterization of foreign materials in paraffin-embedded pathological specimens using in situ multi-elemental imaging with laser spectroscopy, Mod. Pathol. 31 (2018) 378-384.

[17] M. Bonta, J.J. Gonzalez, C.D. Quarles, R.E. Russo, B. Hegedus, A. Limbeck, Elemental mapping of biological samples by the combined use of LIBS and LA-ICP-MS, J. Anal. At. Spectrom. 31 (2016) 252-258.

[18] A. Moussaron, S. Vibhute, A. Bianchi, S. Gunduz, S. Kotb, L. Sancey, V. Motto-Ros, S. Rizzitelli, Y. Cremillieux, F. Lux, N.K. Logothetis, O. Tillement, G. Angelovski, Ultrasmall Nanoplatforms as Calcium-Responsive Contrast Agents for Magnetic Resonance Imaging, Small 11 (2015) 4900-4909.

[19] M. Abdelhamid, F.J. Fortes, M.A. Harith, J.J. Laserna, Analysis of explosive residues in human fingerprints using optical catapulting–laser-induced breakdown spectroscopy, J. Anal. At. Spectrom. 26 (2011) 1445-1450.

[20] Y. Gimenez, B. Busser, F. Trichard, A. Kulesza, J.M. Laurent, V. Zaun, F. Lux, J.M. Benoit, G. Panczer, P. Dugourd, O. Tillement, F. Pelascini, L. Sancey, V. Motto-Ros, 3D Imaging of Nanoparticle Distribution in Biological Tissue by Laser-Induced Breakdown Spectroscopy, Sci. Rep. 6 (2016) 29936.

[21] S. Moncayo, L. Duponchel, N. Mousavipak, G. Panczer, F. Trichard, B. Bousquet, F. Pelascini, V. Motto-Ros, Exploration of megapixel hyperspectral LIBS images using principal component analysis, J. Anal. At. Spectrom. 33 (2018) 210-220.

[22] S. Pagnotta, M. Lezzerini, L. Ripoll-Seguer, M. Hidalgo, E. Grifoni, S. Legnaioli, G. Lorenzetti, F. Poggialini, V. Palleschi, Micro-Laser-Induced Breakdown Spectroscopy (Micro-LIBS) Study on Ancient Roman Mortars, Appl. Spectrosc. 71 (2017) 721-727.

[23] V. Motto-Ros, D. Syvilay, L. Bassel, E. Negre, F. Trichard, F. Pelascini, J. El Haddad, A. Harhira, S. Moncayo, J. Picard, D. Devismes, B. Bousquet, Critical aspects of data analysis for quantification in laser-induced breakdown spectroscopy, Spectrochim. Acta Part B 140 (2018) 54-64.

[24] E. Képeš, P. Pořízka, J. Klus, P. Modlitbová, J. Kaiser, Influence of baseline subtraction on laser-induced breakdown spectroscopic data, J. Anal. At. Spectrom. 33 (2018) 2107-2115.

[25] M.D. Dyar, S. Giguere, C.J. Carey, T. Boucher, Comparison of baseline removal methods for laser-induced breakdown spectroscopy of geological samples, Spectrochim. Acta Part B 126 (2016) 53-64.

[26] J. El Haddad, L. Canioni, B. Bousquet, Good practices in LIBS analysis: Review and advices, Spectrochim. Acta Part B 101 (2014) 171-182.

[27] F. Trichard, L. Sorbier, S. Moncayo, Y. Blouët, C.P. Lienemann, V. Motto-Ros, Quantitative elemental imaging of heterogeneous catalysts using laser-induced breakdown spectroscopy, Spectrochim. Acta Part B 133 (2017) 45-51.

[28] J. Klus, P. Mikysek, D. Prochazka, P. Pořízka, P. Prochazková, J. Novotný, T. Trojek, K. Novotný, M. Slobodník, J. Kaiser, Multivariate approach to the chemical mapping of uranium in sandstone-hosted uranium ores analyzed using double pulse Laser-Induced Breakdown Spectroscopy, Spectrochim. Acta Part B 123 (2016) 143-149.

[29] R.R.V. Carvalho, J.A.O. Coelho, J.M. Santos, F.W.B. Aquino, R.L. Carneiro, E.R. Pereira-Filho, Laser-induced breakdown spectroscopy (LIBS) combined with hyperspectral imaging for the evaluation of printed circuit board composition, Talanta 134 (2015) 278-283.

[30] M.A. Sperança, F.W.B. de Aquino, M.A. Fernandes, A. Lopez-Castillo, R.L. Carneiro, E.R. Pereira-Filho, Application of Laser-Induced Breakdown Spectroscopy and Hyperspectral

Images for Direct Evaluation of Chemical Elemental Profiles of Coprolites, Geostan. Geoanal. Res. 41 (2017) 273-282.

[31] C.D. Quarles, J.J. Gonzalez, L.J. East, J.H. Yoo, M. Morey, R.E. Russo, Fluorine analysis using Laser Induced Breakdown Spectroscopy (LIBS), J. Anal. At. Spectrom. 29 (2014) 1238-1242.

[32] V. Motto-Ros, E. Negre, F. Pelascini, G. Panczer, J. Yu, Precise alignment of the collection fiber assisted by real-time plasma imaging in laser-induced breakdown spectroscopy, Spectrochim. Acta Part B 92 (2014) 60-69.

[33] E. Tognoni, G. Cristoforetti, Signal and noise in Laser Induced Breakdown Spectroscopy: An introductory review, Opt. Laser Technol. 79 (2016) 164-172.

[34] G.L. Long, J.D. Winefordner, Limit of Detection A Closer Look at the IUPAC Definition, Anal. Chem. 55 (1983) 712A-724A.

[35] J.-M. Mermet, Limit of quantitation in atomic spectrometry: An unambiguous concept?, Spectrochim. Acta Part B 63 (2008) 166-182.

[36] L. Sancey, S. Kotb, C. Truillet, F. Appaix, A. Marais, E. Thomas, B. van der Sanden, J.P. Klein, B. Laurent, M. Cottier, R. Antoine, P. Dugourd, G. Panczer, F. Lux, P. Perriat, V. Motto-Ros, O. Tillement, Long-term in vivo clearance of gadolinium-based AGuIX nanoparticles and their biocompatibility after systemic injection, ACS nano 9 (2015) 2477-2488.